Bio-Synthesized Silver Nanoparticles Using *Pongamia Pinnata* (Pongam) Leaves Extract as Effective Catalyst for the Dilapidation of Rhodamine-B Dye

D. Sujatha[1], A. Alvin Kalicharan[2*], G Ushanandhini[3], K.Arivalagan[4]

[1,4]Department of Chemistry, Government Arts College for Men(A) ,Chennai-600035, India

[2*]Department of Chemistry, Panimalar Engineering College, Chennai-600123, India.

[3]Department of Chemistry, SRM Institute of Science and Technology, Ramapuram Campus, Chennai, India.

*Corresponding Author: A. Alvin Kalicharan

Abstract

This study examined the Rhodamine B (RhB) dye's ability to bind newly synthesised silver nanoparticles (AgNPs) made from the leaves extract of *Pongamia Pinnata(*Pongam*)* RhB removal was examined for the possessions of exchange period, original pH, opening colorant concentration, adsorbent dosage, and temperature, all of which had a big impact on its uptake. Then, prepared AgNPs were examined using TEM analysis, X-ray powder diffraction (XRD). Field-emission scanning electron microscopy (FESEM), Fourier transforms infrared (FT-IR) spectra, and Brunauer-Emmet-Teller (BET). High surface area, with a middling of 0.9208 m^2/g, was found by BET analysis, supporting its use as an effective adsorbent. Utilizing the Temkin, Langmuir and Freundlich, isotherm models, adsorption isotherms were assessed. The Freundlich isotherm, which has an R^2 of 0.9912 and indicates multilayer adsorption, provided the best portrayal of the adsorption process. The rate of adsorption were better designated by pseudo-second-order kinetics, and it was revealed that the adsorption process was controlled by both surface adsorption and intra-particle diffusion. Denoting an exothermic and spontaneous adsorption process comprised of thermodynamic parameters with negative values for $\Delta H°$, $\Delta S°$ and $\Delta G°$.

INTRODUCTION

Today, the substantial fraction of developing nations with less strict laws face major obstacles in providing their populations with sustainable, high-quality drinking water even though their natural water sources are increasingly endangered from man-made pollution and agricultural and industrial effluents. Large quantities of water are frequently used in dye-related chemical reactions and products (e.g. textile, leather, paints, paper and pulp manufacturing, cloth dyeing, leather treatment, and printing). Owing to the existence of many synthetic or natural colouring pollutants, such as acids, bases, dissolved solids, hazardous chemicals, and pigments, water treatment or recovery is challenging. In addition to being unsightly, coloured substances in water and wastewater prevent light from entering ponds, which interferes with the biological treatment process inside the treatment plant [1], [2]. Additionally, a lot of dyes are hazardous to certain kinds of bacteria, which can either directly destroy them or hinder their ability to catalyse [3].

In the paper printing, paint, textile dyeing, and leather industries, cationic dye Rhodamine B is frequently employed. To safeguard the water, the environment, and the general public's health, the dye must be removed from the sewage. Because they have the bioaccumulation property, dyes have a toxic effect that is not limited to plants but also has the same effect as a carcinogen on people and animals [4].

Filtration, chemical coagulation, biological oxidation, active sludge, solvent extraction, photo degradation, flocculation, and adsorption are just a few of the technologies that have been engaged to eradicate colours from tainted wastewaters [5, 6]. Owing to its great efficiency, low cost, and simplicity of use, the adsorption technique has garnered researchers' interest recently [7]. As adsorbents materials are many types such as zeolites, oxides, soil minerals, and carbon compounds have been used. In any event, there are still a few problems that restrict users, like that adsorption ratio not being high enough and the

adsorbent being difficult to separate. Finding novel adsorbents to address these issues is therefore of great interest [8].

Metal nanoparticles are increasingly being used as adsorbents because of their shape, which includes highly reactive sites, regulated size, and large surface area. Metal nanoparticles and /metal oxide nanoparticles (NPs) such platinum, strontium, silver, and zinc oxide were added to oxide of graphene (GO) nanosheets, and it was shown that this improved their ability to adsorb substances as well as their antibacterial, electrical conductivity, and photocatalytic properties. In comparison to other metals, AgNPs have drawn a lot of attention from researchers, particularly in the fields of biomedicine, sensors, and catalysts [9-16]. This is because AgNPs have excellent qualities like high electrical conductivity, antibacterial properties, and dye uptake capacity.

Figure 1. Image of *Pongamia Pinnata(Pongam)* leaves

From this vantage point, it is unblemished that the blend of AgNPs in general frequently involves the use of dangerous chemicals, but growing environmental concerns have prompted researchers to look for more eco-friendly preparation techniques. The *Pongamia Pinnata(Pongam)* leaves Extract is one of the potential precursors that may be utilised to create nanoparticles from metal salt solutions and serves as an excellent nanofactory. It had been discover that this plant has excellent pharmacological qualities, including antiplasmodial [17], antifungal [18], anticancer [19], antioxidant [20], and antimicrobial activity [21].

Given their highly maximum surface energy during the preparation process, AgNPs are known to aggregate

quickly. To remove Rhodamine B dye since industrial effluents, we disclosed in this study a simple method for synthesising AgNPs utilising an extract from *Pongamia Pinnata(Pongam)* leaves. Additionally, it is shown that the produced adsorbent may be used successfully in a real water treatment progression by methodically elucidating the stability, kinetics, and mechanism of dye adsorption.

2. RESOURCES AND TECHNIQUES
2.1 Resources
Fresh leaves of *Pongamia Pinnata(Pongam)* were procured in Panimalar Engineering College, Tamilnadu. Analytical grade sample of AgNO$_3$ (Silver Nitrate), NaOH, Ethanol (C$_2$H$_5$OH) was used without any additional purification in addition to deionised water.

2.2 Techniques
2.2.1 Forging of *Pongamia Pinnata(Pongam)* Leaves Extract
Fresh *Pongamia Pinnata(Pongam)* Leaves are collected and then washed persistently with tap water and again by distilled water to clear out the dust. The clean, fresh leaves are pulverised in a professional blender after drying at room temperature for 6 to 11 days in an enclosed location. The fine particles are reserved at room temperature until needed. 10 grams of leaf extract powder were placed in a 250 ml conical flask, to which 100 ml of double distilled water was added and boiled at 80°C for 30 minutes. The solution was then strained through Whatman filter paper and set aside for the next step. The resulting Concentrate was pale brown in colour and had a pH of 11 due to the addition of 0.1M sodium hydroxide solution.

2.2.2. Preparation of Silver Nanoparticles (Adsorbent)
In a 250 ml conical flask, 50 ml of *Pongamia Pinnata(Pongam)* leaves Extract was placed, and 100 ml of 0.1 M AgNO$_3$ solution was gradually added at room temperature under static conditions. The colour change was observed, as well as the time it took for the reaction to occur. The colour of the solution changes from pale brownish to reddish-brown as silver nanoparticles (AgNPs) form. The solution is then centrifuged, and the precipitate is concentrated and dried in an electrical oven at 100°C for 24 hours. Green synthesised AgNPs are formed with uniform particle size and stored for future characterization and applications.

2.2.3 Preparation of Rhodamine B (RhB) (Adsorbate)

Sigma-Aldrich Chemicals in Chennai supplied the synthetic colour Rhodamine B (RhB). By dissolving 1.0 g of dye in distilled water, a store solution of (1000mg/L) was prepared. All of the solutions and reagents were made with distilled water. Figure 2. Shown in chemical structure of Rhodamine B (RhB).
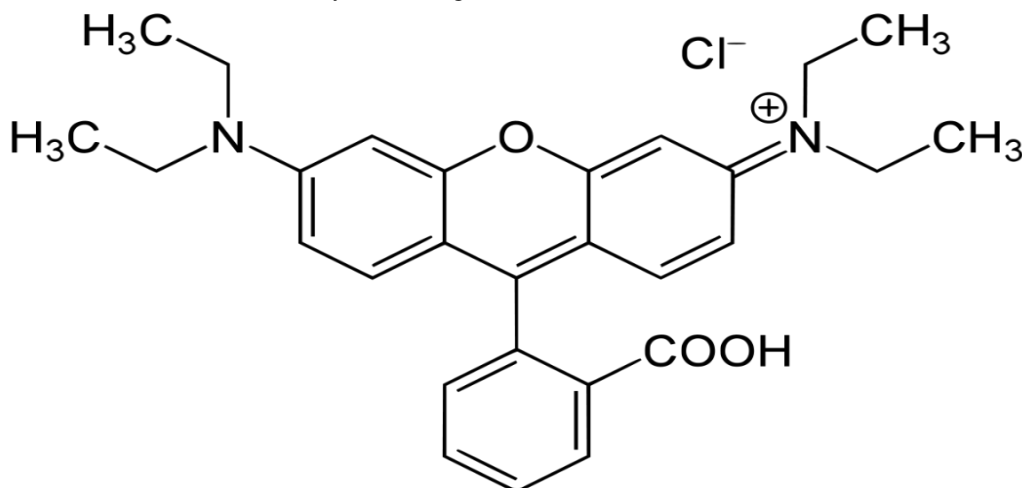
Figure 2. Chemical Structure of Rhodamine B

2.3 Delineation of Silver Nano-particles

2.3.1 UV-Visible spectrophotometric analysis

UV-Visible spectroscopic analysis of sequenced Ag nanoparticles confirmed the early onset of nanoparticle generation. An Elico SL210 UV-Visible Spectrophotometer, the scanning range between the 190 nm to 800 nm which examines the resulted Ag Nano-particles.

2.3.2 FT-IR Spectroscopic analysis

The FT-IR spectrometer was harnessed to interpret the functional group of the plant Concentrate and biogenically engendered Ag Nano-particles. The study of peaks at particular wave numbers is the underpinning of spectroscopic method. According to FT-IR data, both the plant Concentrate and the produced Nano-particles manifest the available functional groups. Utilizing Perkin Elmer equipment, the frequency range of FT-IR characterization was the 400 and 4000 cm^{-1}.

2.3.3 X-ray diffraction analysis (XRD)

The crystallite structure and mean size of the particle of the procured adsorbent particles were scrutinized. XRD pattern was measured by X-ray diffractometer (BRUKER D8 ADVANCE) of characteristics CuK radiation (λ=1.541Å) in the assortment 4º to 80º at a scan rate of 0.02º per/min with time constant of 2 minutes.

2.3.4. Scanning Electron Microscopy (SEM)

The porosity, particle size spreading of the adsorbents is all detailed by the SEM investigation. Using JEOL-6390LA paraphernalia, the surface morphology of biosynthesised AgNP's was apprehended.

2.3.5 Transmission Electron Microscopy (TEM)

For ascertaining the particle measurement and morphological congruence of AgNP's and other metal nano-particles, TEM (JEOL –JEM 2100) is encouraged as the best electron microscopy technique.

2.3.6 Dynamic Light Scattering (DLS)

The middling size of the fabricated AgNPs was determined using DLS (Spectroscatter 201).

2.3.7 BET analysis

The BET specific surface areas were measured from the N$_2$ desorption and adsorption isotherms at 77 K composed by a Quanta chrome Autosorb-6B outward zone and pore size analyser. Previously every dimension, fresh HTs were first degassed at 100 ºC overnight.

2.3.8 Batch adsorption experiments

The batch adsorption approach was used for the experiment. The elimination of Rhodamine B dye was investigated by the lot routine at many temperatures (298K, 308K, 318K, and 328K) to appraise the outcome of operational parameters likewise pH, contact time, adsorbent dosage, initial dye concentration and solution temperature. The isotherm investigation was performed with dyes ranging in

concentration since 10 to 50mg/L that were meticulously organised in an orbital shaker and agitated at 150rpm for 30 minutes. For improved adsorption, the adsorbent dosage was varied from 0.2 to 1.0g. The kinetic examination was complete by adjusting the time from 30 to 150 minutes, although the thermodynamic study was done by varying the temperature from 298 to 328K. Centrifugation at 2000rpm for 10 minutes separated the AgNPs solution. Residual concentration of dye was determined UV-visible spectrophotometer at respective wavelength. The percentage of dye elimination from solution was calculated following

The percentage of Rhodamine B adsorbed was determine founded on the subsequent formula

$$\% \, removal$$
$$= \frac{(Co - Ce)}{Co} X \, 100 \qquad Eq. (1)$$

The maximum RhB uptake q_e (in mg/ g) was calculated as shown below

$$qe$$
$$= \frac{(Co - Ce)V}{M} \qquad Eq. (2)$$

Where C_o and C_e are early and final Rhodamine B concentration of in mg 1^{-1}, respectively W is the weight of AgNP (in g) and V is the volume of RhB solution.

3. RESULTS AND DISCUSSION

3.1. Characterization study of the bio synthesized silver nano-particles

Water-soluble components in *Pongamia Pinnata(Pongam)* leaf Concentrate were performing an important function in the formation of AgNPs from silver monovalent ions. The colour change confirmed preliminary evidence of Nano-particle formation. The homogeneous mixing of leaf Concentrate and aqueous silver nitrate solution turned pale brown to reddish-brown.

3.1.1. UV- Vis Absorption Spectroscopy of Silver Nano-particles.

By employing the concentrate from *Pongamia Pinnata(Pongam)* leaves, the biogenic method for producing Ag Nano-particles was divulged. Metal Nano-particle fabrication in aqueous solution can be confessed by UV-Vis spectroscopy [22]. The UV-Vis spectrum of colloidal solution of AgNP's was exposed in Figure 2a. At 420 nm, a broad band appeared, signifying the production of AgNP's [23-24].

3.1.2 Fourier Transform Infrared (FT-IR) Spectroscopy

The FT-IR study was done to interpret the main functional groups that are present in the *Pongamia Pinnata(Pongam)* leaf concentrate and are in charge of contriving AgNP's (Figure 2b). The mantle of various functional groups in *Pongamia Pinnata(Pongam)* leaves concentrate in the reducing and steadying progressions of nanoparticle fabrication was gauged using the spectrum. Exploration was further done on the absorbance bands at 3635, 2100, 1645, 1380, and 1116 cm^{-1} in leaves Concentrate. The hydroxyl group elements O-H stretching vibration caused a broad band at 3635 cm^{-1}. The peaks at 1645 and 1380 could be attributed to bonds comprising -NH_2 groups of protein amino acids and -C=O groups of flavonoids and tannin respectively. AgNP's peaked at 3431, 2927, 1612, 1103 and 668 cm^{-1}respectively. Flavonoids, other phenolic compounds and xanthonoids, which were thought to be the primary reducing agent for silver ions were found to include OH stretching, as seen by the wider peak at 3338 cm^{-1}.
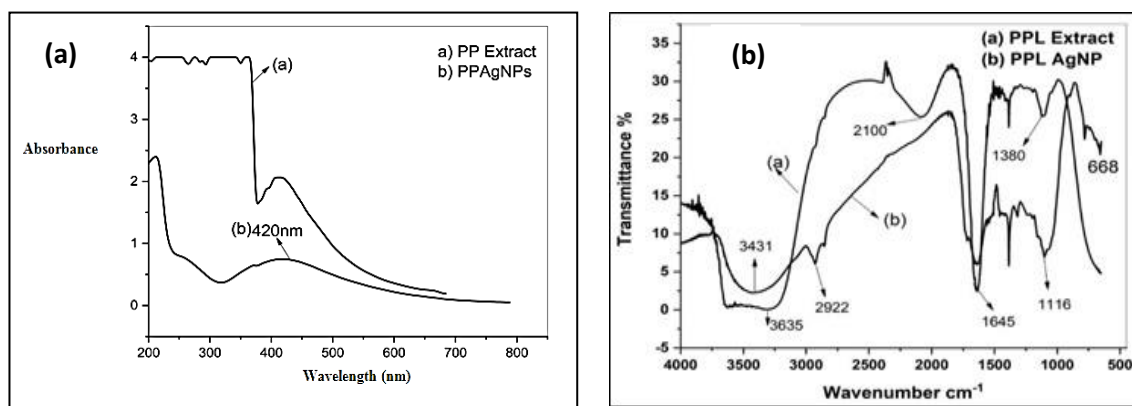
Figure 2: 2(a): UV-Vis spectra of (i) PPLE and (ii) PPLAgNP's and 2(b) FTIR Spectra of a) PPL Concentrate and b) PPLAg NPs

The reduction of the silver ions (Ag+) by OH-based products which were found in leaves is thought to be the reason of the change in OH stretching frequency from higher (in Concentrate) to lower (in Ag NPs) frequency [25–26]. The biomolecule found in the leaf concentrate was in charge of the reduction of silver salt, as evidenced by the production of AgNP's.

3.1.3. X-Ray Diffraction (XRD) Analysis

The X-ray diffraction findings was used to determine and confirm the crystallite structure of the biosynthesized AgNP's (Figure 3) renders the appearance of a diffraction pattern at $2\theta = 32.36º$, $38.27º$, $44.31º$, $64.03º$, and $77.83º$ that is in tune to the monoclinic phase AgNP's planes (311), (220), (200) and (111). In the diffraction images, no clear-cut peak caused by any impurity was seen, pointing to the formation of pure crystalline AgNP's. The Debye-Scherer Equation (3) was used to analyse the average size of crystalline AgNP's [27]. AgNP's are confirmed by a strong peak with the (111) plane diffraction at $2\theta = 35.4º$ and $38.27º$. In samples of AgNP's, the average size is less than 21 nm.

$$D = k\lambda/\beta\cos \quad Eq.\,(3)$$

Where, k represents shape factor and is about to be 0.89. θ is the diffraction angle, β denotes full width at half maximum, and λ denotes wavelength of X-ray radiation (0.154 nm). The standard crystallite measurement was estimated about to 24.84 nm in size.
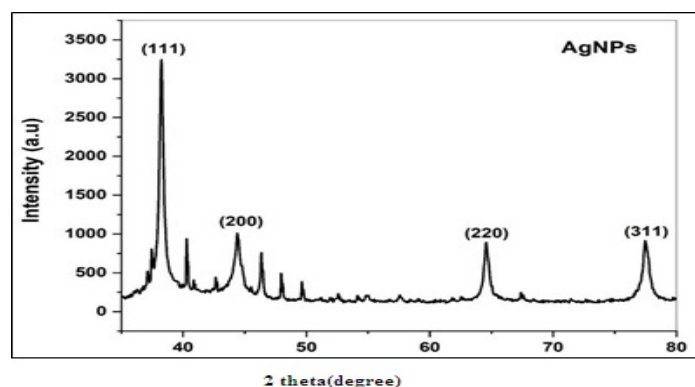
Figure 3. XRD image of Green synthesized Silver Nano-particles

3.1.4 Scanning Electron Microscopy (SEM)

The morphology of the silver nano-particles is displayed in Figure 4a. Affording on the image J program's calculations, the diameter of Ag Nano-particles appears to range between 60 and 160 nm.

3.1.5 Transmission Electron Microscopy (TEM)

Engaging a TEM, the comprehensive morphological and size assessments of eco-friendly produced AgNP's were examined. According to the TEM image (Figure 4b), the biosynthesized AgNP's were agglomerated, and associated to one another, and are spherical in dimension, which is also coherent with the SEM data. The estimated size of AgNP's is observed between 20 and 35 nm.
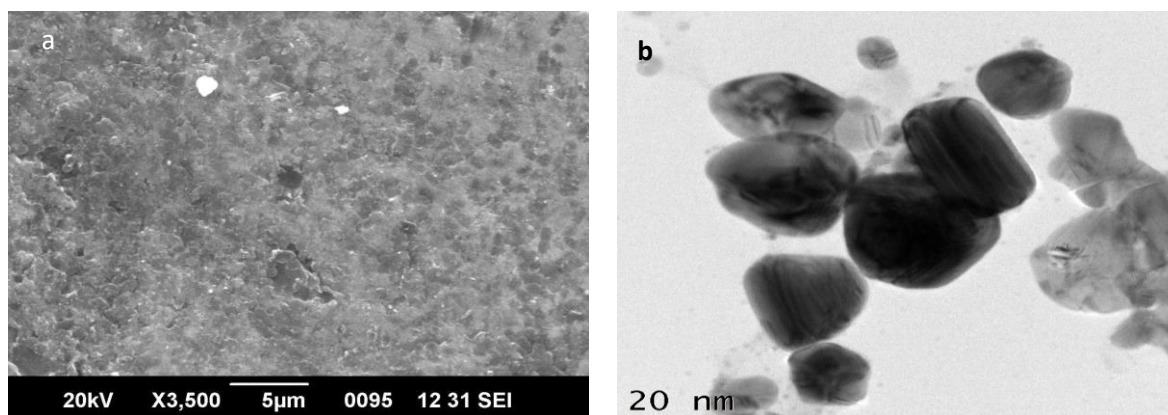
Figure 4. 4(a)SEM image of Bio-synthesized Silver Nano-particles and 4(b) TEM image of Bio synthesized silver Nano-particles.

3.1.6 Dynamic Light Scattering (DLS) Examinations

DLS is the most often applied technique to determine the distribution of AgNP's size in its condensed state. The evaluated result of AgNP's particle size shows the size variation range mendacities amongst 10 and 120 nm with highest size variation around 75.8 nm as shown in Figure 5. Comparatively the size variation diagrams in DLS analysis have good symmetry and reveals the homogeneity of resultant AgNP's.
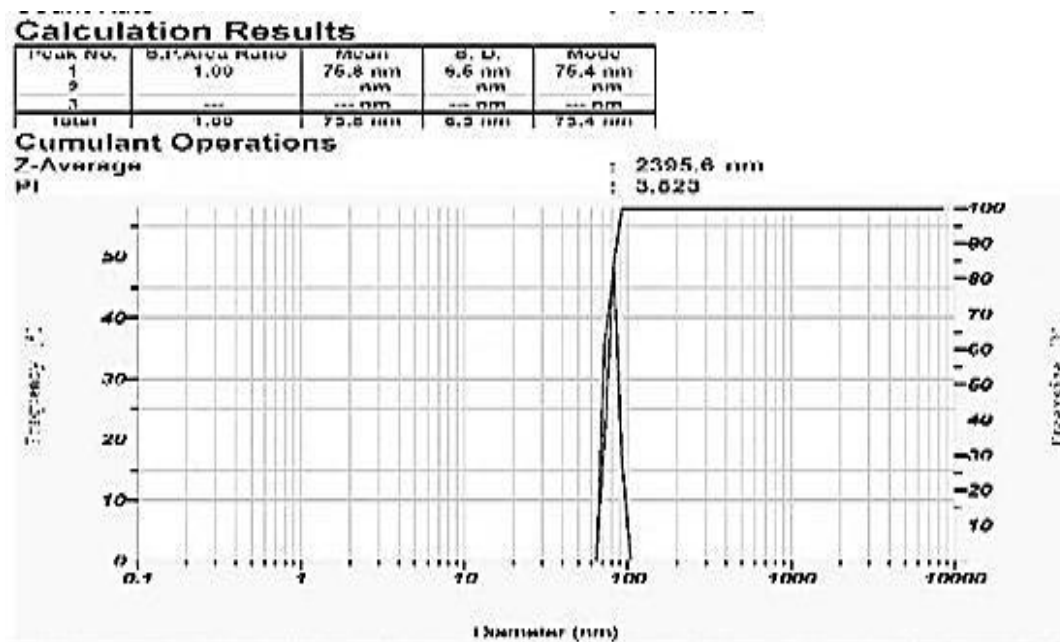
Figure 5. Dynamic Light Scattering Data of AgNP's

3.1.7 BET Analysis

Adsorption, heterogeneous catalysis, and reactions on the surfaces of nanoparticles all rely on specific surface area (SSA). The surface area calculated was 0.9208 m^2/g (Figure 6). A lower surface-to-volume ratio allows for increased catalytic activity. [28].
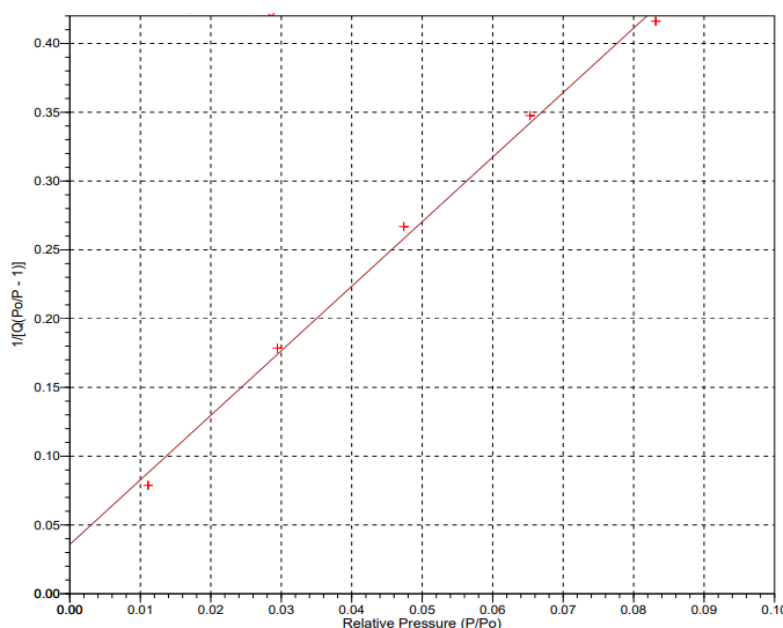
Figure 6. BET analysis data of AgNP's

3.2 Impact of adsorption process parameters on RhB eradication.

3.2.1 Effect of initial dye concentration of RhB

The inference of the initial concentration of RhB in the solutions on the rate of adsorption on AgNPs was investigated. The Experiments parameter was agreed out with static adsorbent dosage optimal pH and stably maintained temperature. The RhB dye removal percentage is plotted against the initial dye concentration shown in Figure 7a. The dye removal percentage is decreased from 99.06to 92.20% with initial dye concentration is increase from 10 to 50 mg/L, Maximum adsorption of 99.06% was recorded for (10mg/L). The outcome indicates that quick initial adsorption on the adsorbent's exterior surface is followed by a gradual inward process of diffusion, which may be the rate-determining phase.

3.2.2 Effect of Adsorbent Dose

The effect of adsorbent dose on the removal of the RhB from aqueous solution was determined using variable quantities of GS-AgNPs adsorbent ranging from 0.2 g to 1.0 g at fixed volumes 50 (ml) with initial dye solution 50 mg/L under constant parameters. The results are shown Figure 7b. The highest percentage of RhB removal was achieved using 0.2g AgNPs. At elevated levels of AgNPs the quantity of RhB removal gets increased. The observed increase in RhB dye removal with increase adsorbent quantity from 86.29% to 99.01%. This phenomenon could be explained by the fact that increasing the dosage of the adsorbent increases the surface area, which creates more active sites for binding dye from the aqueous phase.

Figure 7. 7(a) The plot of Initial RhB dye concentration Vs % Dye removal on the adsorption of GS-AgNPs. **7(b).** Effect of adsorbent dose on removal of RhB, **7(c)** Effect pH on the adsorption of RhB onto GS-AgNPs, **7(d)** Effect of contact time on the adsorption of RhB onto GS-AgNP.

3.2.3 Effect of pH

To study the effect of initial pH onto adsorption. The pH of RhB solution was varied from 3 to 10. The results of the variation in RhB percentage removal with increase in pH is shown Figure 7c. The highest adsorption was seen at pH 3, and as pH increased from 3 to 10, the % removal of RhB declined from 99.02% to 75.06%. AgNPs' surface was strongly cationic, and RhB's surface was likewise cationic, which led to a low adsorption rate because the adsorbent and the adsorbate were attracted to one another. However, at pH 3, RhB's surface turns anionic, leading to a high

rate of adsorption. This may be because of the favourable RhB adsorption caused by electrostatic interaction between cationic adsorbent and anionic adsorbate. [29, 30]

3.2.4 Effect of contact time

To identity the effect of contact time an experiment was conducted by mixing 50 ml of Rhodamine B solution 50 mg/l concentration with 1g of GS-AgNPs adsorbent at constant pH 3 with varying time intervals of (30,60,90,120 and 150) minutes respectively. The contact time effect on the Rhodamine B adsorption onto GS-AgNPs is depicted in Figure 7d. It is

hypothesized that the initial, quick dye adsorption was caused by the abundance of empty sites on the adsorbent surface, which steadily diminished over the course of the adsorption process until all potential sites were taken up. At that point, the adsorbent and the dye are in equilibrium.

3.2.5 Effect of temperature
Temperature is vital factors that sway dye adsorption the upshot of temperature on the dye (Rhodamine B)

removal percentage onto GS-AgNPs is shown in Figure 8a. The % removal adsorption decreased from 99.01% to 98.16% with the temperature increased from 298K to 328K. . This demonstrates the exothermic nature of the adsorbent-based RhB dye adsorption process. The physical interactions between the dye molecule and the active sites of the adsorbent may weaken as temperature rises, decreasing the efficacy of the adsorption process. [31]
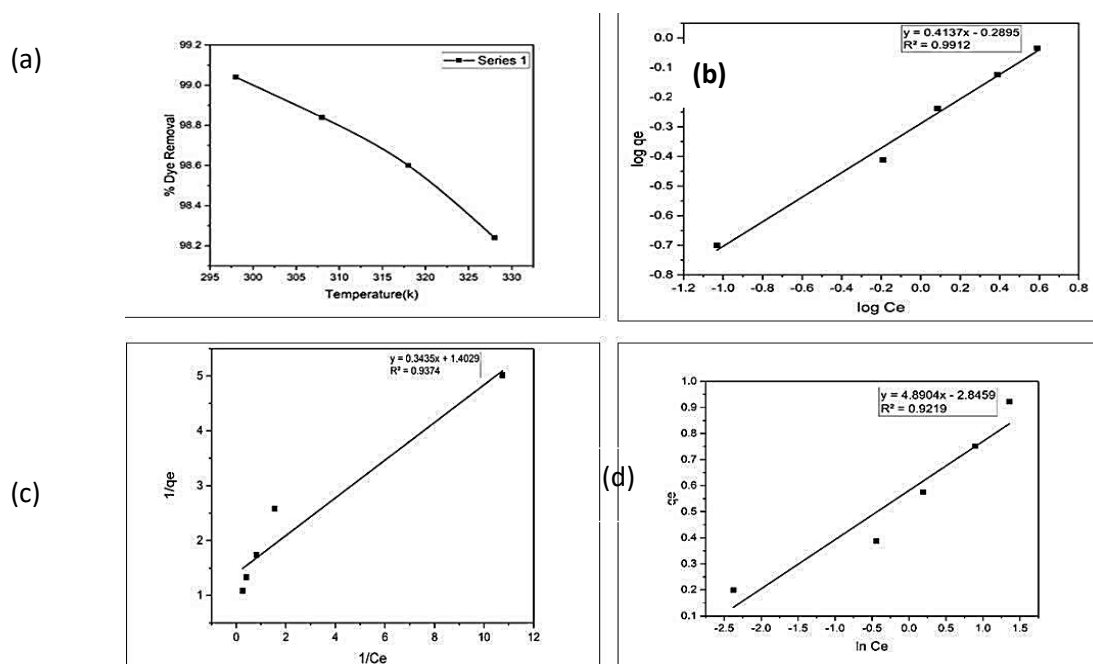
Figure 8.8(a) Effect of temperature on the adsorption of RhB onto GS-AgNP, **8(b)** Freundlich isotherm plot for the adsorption of RhB against 1 g of AgNPs, **8(c)** Langmuir isotherm plot for the adsorption of RhB onto 1 g of AgNPs, **8(d)** Temkin isotherm plot for the adsorption of Rhodamine-B onto 1 g of AgNPs

3.3 Adsorption Isotherms in correlation with RhB dye removal
It is expected that the RhB dye adsorption capability of on AgNPs should correlate with Freundlich, Langmuir and Temkin isotherms.

3.3.1 Freundlich Adsorption Isotherm
The Freundlich isotherm model is based on adsorption on a assorted surface and adopts the adsorption that occurs at active sites of the adsorbent with a different energy. [32]

The equation is generally written as:

$$\text{Log qe} = \log K_F + \frac{1}{n} \log Ce$$
$$Eq.\,(4)$$

K_F is Freundlich constant (mg/g) and n is connected to the adsorption capability and intensity. The model parameters n and the equipoise adsorption capability was estimated by plotting log Ce versus log qe is shown in Figure 8b Value of K_F and n were

determined and are given in Table 1 which shows that an increase in the negative charge on the surface, increases the electrostatic force like vanderwaal's force between the AgNPs, in turn, increases the adsorption of RhB.

3.3.2. Langmuir Adsorption Isotherm
Langmuir model is based on the intermolecular forces that decrease rapidly with distance and the predicted monolayer sorption of the adsorbate on the active site of the adsorbent.

Langmuir isotherm is expressed in the following equation

$$\frac{1}{qe} = \frac{1}{qm\,Kl\,Ce} + \frac{1}{qm} \qquad Eq.\,(5)$$

Ce is the adsorbate concentration at equilibrium (mg/L), q_e is the amount of adsorbed dye per gram of adsorbent (mg/g), K_L is the Langmuir equilibrium constant and q_m (mg/g) is monolayer adsorption capacity. Value of q_m and K_L were calculated from the

slope and intercept of the plot of Ce/qe versus Ce. Langmuir isotherm plots for Rhodamine B on AgNPs are presented in Figure 8c. Langmuir isotherm parameters are presented in Table 1.

From the results, it was perceived that the appropriate nature of the above-stated isotherm model proposes that both homogeneous and heterogeneous sites are intricate in accomplishing the procedure of adsorption.[33]

3.3.3 Temkin Adsorption Isotherm

The temkin adsorption isotherm is given as

$$qe = B \ ln \ ln \ KT + B \ \ ln \ ln \ Ce$$
$$Eq. (6)$$

KT is the Temkin isotherm constant (L/g), B (J/mole) corresponds to the binding energy at its maximum and constant analogous to the heat of adsorption. Determination of the constant KT and B was obtained from a plot between qe and ln Ce (Figure 8d) shows the intercept and slope respectively. The results of the plot are given in Table 1. It is observed that constants KT and B are high for good adsorbents and low for poor adsorbents [34]. Thus adsorption of Rhodamine-B obeys Temkin isotherm reasonably well.

Table 1. Adsorption Isotherm parameters for Rhodamine B dye

Adsorption Isotherm	Parameters	Obtained values
Freundlich Isotherm	K_F (mg/g)	0.5132
	1/n	2.1477
	n	0.4136
	R^2	0.9912
Langmuir Isotherm	K_L (mg^{-1})	4.0849
	q_m (mg/g)	0.2448
	R_L	0.0238
	R^2	0.9374
Temkin Isotherm	K_T (mol/g)	0.1793
	B_T (mol/kJ)	4.8904
	R^2	0.9219

3.4   Adsorption Kinetics

The kinetics of adsorption was investigated by the pseudo-first-order and pseudo-second-order kinetic equations.

3.4.1 Pseudo First Order Model:

The pseudo-first order equation of Lagergren is generally expressed as follows:

$$\log (qe - qt) = \log(qe) - k_1/2.303t \text{-------- } Eq(7)$$

Where qe and qt are the sorption capacities at equilibrium and at time t, respectively (mg g−1) and k_1 (min−1) is the rate constant. [35]

k_1 at 25 °C was calculated from the slope of the plot between log (qe – qt) versus t and qe from the intercept and these data's are listed in the Table 2.[Figure 9a].
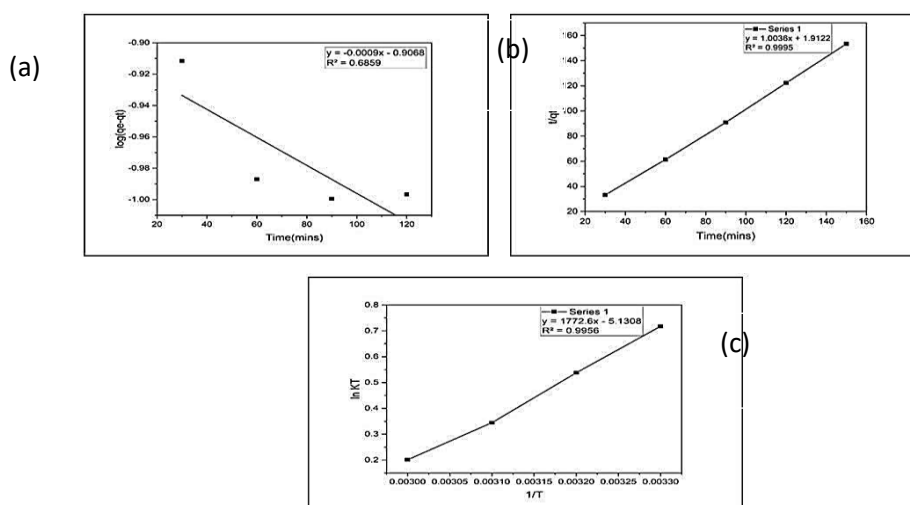
Figure 9. 9(a) Pseudo First Order Kinetic Model of RhB on AgNPs, **9(b)** Pseudo Second Order Kinetic Model of RhB on AgNPs and **9(c).** Plot of ln KT against reciprocal temperature for RhB sorption onto AgNPs

3.4.2 Pseudo Second Order Model:

The pseudo-second order equation of Lagergren is generally expressed as follows:

$$t/qt = 1/K_2\, q_e^2 + t/q_e \qquad\qquad Eq.(8)$$

Where qe and qt are the sorption capacities at equipoise and at time t, respectively (mg g−1) and k_2 is the rate constant of pseudo second-order sorption (g mg−1 min−1). [36]

qe and k_2 values are determined by the slope and intercept of the straight line of the linear plot t/qt versus t and listed in Table 2.[Figure 9b].

Hence, the experiment data showed good accordance with pseudo second-order model in terms of high correlation coefficient values, indicating that the rate-controlling step of chemisorption's was probably the valence forces produced by sharing or exchange of electrons between adsorbent and adsorbate

Table 2. Adsorption Kinetics parameters for RhB

Adsorption Kinetics	Parameters	RhB (Obtained Values)
Pseudo First Order	k_1 (min^{-1})	0.0697
	q_e (mg g^{-1})	5.8036
	R^2	0.6029
Pseudo Second Order	k_2 (g^{-1} mg^{-1} min^{-1})	0.1286
	q_e (mg g^{-1})	1.1435
	R^2	0.9950

.

3.5 Adsorption thermodynamics

The Rh B adsorption process was conducted at different temperatures between 25°C and 55°C. The thermodynamic parameters such as free energy change (ΔG°), enthalpy change (ΔH°) and entropy change (ΔS°) of adsorption were determined using the following equations:

$$\Delta G^\circ = -RT\ln K \qquad Eq.(9)$$
$$\log K = \Delta S^\circ/2.303\,R - \Delta H^\circ/2.303\,RT \qquad Eq.(10)$$
$$\Delta G^\circ = \Delta H^\circ - T\Delta S^\circ \qquad Eq.(11)$$

R was the gas constant (J/mol K); T was the absolute temperature in Kelvin; ΔH° (kJ/mol) and ΔS° (kJ/mol)

could be calculated from the slope and intercept of the linear plot of ln Kt versus 1/T; and ΔG° was calculated. [Figure 9c]

The values of ΔH°, $\Delta S°$ and ΔG° that obtained from the linear plots of ln kt versus 1/T, were summarized in Table 3. The ΔH° of Rh B adsorption on AgNPs was negative, indicating that the adsorption was an exothermic process in nature. The negative value of ΔG° demonstrated the spontaneity and feasibility of the adsorption process of Rh B on the active sites of AgNPs. Moreover, the positive value of ΔS° confirmed the increased randomness at the solid–liquid interface during the adsorption of Rh B. [37]

Table 3. Thermodynamic Parameters for Rhodamine B dye

Dye	Temperature (K)	ΔG^o (J.mol^{-1})	ΔH^o (KJ.mol^{-1})	ΔS^o (J.mol^{-1}.K^{-1})	R^2
RhB	298	-1.8031	-33.940	98.24	0.9956
	308	-1.3678			
	318	-.9110			
	328	-0.5489			

4. Conclusion

In this study, we used *Pongamia Pinnata(Pongam)* leaf extract to produce silver nanoparticles via a biogenic method. For green production of AgNPs, the leaf extract worked as a reducing and stabilizing agent. The physiochemical physiognomies of the produced AgNPs were deliberate using UV-Vis, FTIR, XRD, DLS, SEM, TEM, and SAED techniques. The SPR phenomena was observed using UV-Vis spectroscopy, exhibiting an absorbance peak at 426 nm. During the synthesis protocol, the evident colour change from pale brown to reddish-brown confirms the creation of

AgNPs. The functional groups adhering to the apparent of AgNPs were identified using FTIR. The average size of AgNps predicted to be 24.84 nm using Debye Scherrer's equation. A single peak in the DLS plot confirms the excellent purity of the amalgamated silver nanoparticles. The shapes of AgNPs have shown in spherical in shapes. This demonstrated by microscopic methods. The bright dots in the SAED pattern indicated the AgNPs strong crystallinity. We investigated the degradation of RhB dye using various parameters such as dye concentration, adsorbent dose, pH, contact time, and temperature. We discovered that

the best reaction conditions for successful RhB dye removal are 10 mg dye with 1.0 g of adsorbent at pH=3 within 90 minutes contact time and at 298 K temperature. The pseudo-second-order kinetic model fit the equilibrium adsorption data excellently. Fitting the data to the Temkin, Langmuir and Freundlich models are leads to a greater correlation coefficient with R^2 of 0.9912 for the Freundlich isotherm. A negative value for $\Delta G°$ proposes that the adsorption is spontaneous. The recent results conclude that *Pongamia Pinnata(Pongam)* leaf extract biosynthesized AgNPs are a cost-effective and environmentally benign adsorbent that can be used as an alternative nanomaterial to the existing pricey materials used for dye removal from aqueous solutions.

Conflict of Interest
The author declares that there is no conflict of interest.

References:
1. McKay, G, Adsorption of dyestuffs from aqueous solutions with activated carbon I: Equilibrium and batch contact-time studies,1984. *J. Chemi.Tech. And Biotech*. 34, 294–310.
2. Asfour, H.M, Nassar M.M, Fadali O.A and El-Guendi, M.S, Colour removal from textile effluents using hardwood sawdust as an absorbent, 1985. *J. Chemi.Tech. and Biotech*, 35, 28– 35.
3. Chu, W, Dye Removal from Textile Dye Wastewater Using Recycled Alum Sludge, 2001. *Water Research*, 35, 3147–3152.
4. Shah. J., Jan. M. R., Haq A. and Khan Y., Removal of Rhodamine B from aqueous solutions and wastewater by walnut shells: Kinetics, equilibrium and thermodynamics studies., 2013. *Frontiers of Chem. Sci. Eng,* 7, 428-436.
5. Ayad M. M. and Abu El-Nasr. A.*,* Adsorption of Cationic Dye (Methylene Blue) from Water Using Polyaniline Nanotubes Base., 2010. *J. Phys. Chem. C*, 114, 14377-14383.
6. Wong Y. C., Szeto Y. S., Cheung W. H. and McKay. G., Equilibrium Studies for Acid Dye Adsorption onto Chitosan., 2003. *Langmuir*, 19, 7888-7894.
7. Sivakumar. P and Palanisamy P. N., Adsorption Studies of Basic Red 29 by a Non-Conventional Activated Carbon Prepared from Euphorbia Antiquorum, 2009. *Int. J. Chem.Tech. Res,* 1, 502-510.
8. Shahabuddin. S., Muhamad Sarih N., Mohamad S. and Joon Ching J., $SrTiO_3$ Nanocube-Doped Polyaniline Nanocomposites with Enhanced Photocatalytic Degradation of Methylene Blue under Visible Light., 2016. *Polymers (Basel.)*, 8, 27.
9. Shahabuddin S., Sarih N., Afzal Kamboh M., Rashidi Nodeh H. and Mohamad S., Synthesis of Polyaniline-Coated Graphene Oxide@$SrTiO_3$ Nanocube Nanocomposites for Enhanced Removal of Carcinogenic Dyes from Aqueous Solution., 2016. *Polymers*, 8(9), 305;
10. Song B., Zhang C., Zeng G., Gong J., Chang Y. and Jiang Y., Antibacterial properties and mechanism of graphene oxide-silver nanocomposites as bactericidal agents for water disinfection., 2016. *Arch. Biochem. Biophy*, 604, 167–176.
11. Park, J.Y. and Kim, S., Preparation and electroactivity of polymer functionalized graphene oxide-supported platinum nanoparticles catalysts, 2013. *Int. J. Hydrogen Energy*, 38 , 6275–6282.
12. Atchudan R., Edison T.N.J.I., Perumal S., Karthikeyan D. and Lee Y.R., Facile synthesis of zinc oxide nanoparticles decorated graphene oxide composite via simple solvothermal route and their photocatalytic activity on methylene blue degradation, 2016. *J. Photochem. Photobiol. B Biol,* 162, 500–510.
13. Shahabuddin, S., Sarih N.M., Ismail, F.H., Shahid, M.M., and Huang, N.M., Synthesis of chitosan grafted-polyaniline/Co_3O_4 nanocube nanocomposites and their photocatalytic activity toward methylene blue dye degradation., 2015. *RSC Adv*, 5, 83857–83867.
14. Kumar S., Raj S., Jain S. and Chatterjee K., Multifunctional biodegradable polymer nanocomposite incorporating graphene-silver hybrid for biomedical applications., 2016. *Mater. Des,* 108, 319–332.
15. Bahrami S., Abbasi A.R., Roushani M., Derikvand Z. and Azadbakht A., An electrochemical dopamine aptasensor incorporating silver nanoparticle, functionalized carbon nanotubes and graphene oxide for signal amplification., 2016. *Talanta*, 159, 307–316.
16. Sreekanth T.V.M., Jung M.J. and Eom I.Y.*,* Green synthesis of silver nanoparticles, decorated on graphene oxide nanosheets and their catalytic activity., 2016. *Appl. Surf. Sci*, 361, 102–106.
17. Singh N., Kaushik N.K., Mohanakrishnan D., Tiwari S.K. and Sahal D., Antiplasmodial activity of medicinal plants from Chhotanagpur plateau, Jharkhand, India, 2015. *J. Ethnopharmacol*, 165, 152–162.
18. Roy S., Chatterjee P., A non-toxic antifungal compound from the leaves of Catharanthus roseus characterized as 5-hydroxy flavone by UV

spectroscopic analysis and evaluation of its antifungal property by agar-cup method, 2010. *Ind. Crops Prod*, 32, 375–380.

19. Gajalakshmi S., Vijayalakshmi S. and Devi Rajeswari, V., Green synthesis of Zn-doped *Catharanthus Roseus* nanoparticles for enhanced anti-diabetic activity, 2013. *Int. J. Pharma Biol. Sci*, 4, 821–830.

20. Pereira D.M., Faria J., Gaspar L., Ferreres F., Valentão P., Sottomayor M. and Andrade P.B., Exploiting Catharanthus roseus roots: Source of antioxidants., 2010. *Food Chem.*, 121, 56–61.

21. Mukunthan K.S., Elumalai E.K., Patel T.N. and Murty V.R., Catharanthus roseus: a natural source for the synthesis of silver nanoparticles, 2011. *Asian Pac. J. Trop. Biomed*, 1, 270–274.

22. Philip. D. Unni, C. Aromal and S.A. Vidhu, Murraya Koenigii leaf-assisted rapid green synthesis of silver and gold nanoparticles, 2011. *Spectrochim. Acta Part A Mol. Biomol. Spectrosc,* 78, 899–904.

23. Jagtap U. and Bapat U.B., Green synthesis of silver nanoparticles using Artocarpus heterophyllus Lam. seed extract and its antibacterial activity., 2013. *Ind. Crop. Prod*, 46, 132–137.

24. Awwad A.M., Salem N.M.and Abdeen A.O., Green synthesis of silver nanoparticles using carob leaf extract and its antibacterial activity, 2013. *Int. J. Ind. Chem,* 4, 29.

25. López - Miranda J.L., Cervantes - Chávez J.A., Hernández - Martínez, A.R., Pérez R., Esparza. R., and Estévez-González. M., Study on the photocatalytic and antibacterial properties of silver nanoparticles synthesized by a green approach, 2019. *Mat. Res. Exp*, 6, 065066.

26. Latha D., Prabu P., Gnanamoorthy G., Sampurnam S., Manikandan R., Arulvasu C., and Narayanan V.., Facile *Justicia adhatoda* leaf extract derived route to silver nanoparticle: synthesis, characterization and its application in photocatalytic and anticancer activity, 2019. *Mat. Res. Exp.,* 6, 045003.

27. Paul S. C, Bhowmik S, Nath M. R, Islam M. S, Paul S. K, Neazi J, Monir T. S. B, Dewanjee S, Salam M. A. Silver Nanoparticles Synthesis in a Green Approach: Size Dependent Catalytic Degradation of Cationic and Anionic Dyes, 2020. *Orient J Chem* ,36(3).

28. Sing K. S. W., Everett D. H., Haul R. A. W., Moscou L., Pierotti R. A., Rouquerol J. and Siemieniewska T., "Reporting Physisorption Data for Gas/Solid Systems with Special Reference to the Determination of Surface Area and Porosity", 1985. *Pure and Applied Chemistry*, 57 (4), 603-619.

29. Majumdar SS, Das SK, Chakravarty R, Saha T, Bandyopadhyay TS, and Guha AK. A study on lead adsorption by Mucor rouxii biomass Desalination, 2015. 251,96–102.

30. Giwa AA, Oladipo MA, and Abdulsalam KA., Adsorption of Rhodamine B from single, binary and ternary dye systems using Sawdust of Parkia biglobosa as adsorbent: isotherm, kinetics and thermodynamics studies, 2015. *J Chem Pharm Res* 7, 454–475.

31. Tan, I.A.W.; Ahmad, A.L. and Hameed, B.H., Optimization of Preparation Conditions for Activated Carbons from Coconut Husk Using Response Surface Methodology., 2008. *J. Hazard. Mater.* 154, 337– 346.

32. Tawfik A. Saleh, and Islam Ali, Synthesis of polyamide grafted carbon microspheres for removal of rhodamine B dye and heavy metals, 2018. *J. Environ. Chem. Eng*. 6, 5361–5368.

33. Karagöz S., Tay T., Ucar S., and Erdem M., Activated carbons from waste biomass by sulfuric acid activation and their use on methylene blue adsorption., 2008. *Biores. Technol.* 99, 6214–6222.

34. Temkin M.I., and Pyzhev V., Kinetics of Ammonia Synthesis on Promoted Iron Catalysts. Acta Physicochimica Acta Physiochim., 1940. 12, 327–356.

35. Malkoc E., Ni(II) removal from aqueous solutions using cone biomass of Thuja orientalis., 2006. *J. Hazard. Mater*, 137, 899–908.

36. Ho Y.S., and Mckay G., Sorption of dyes and copper ions onto biosorbents, 2003. *Process Biochem.* 38, 1047-1061.

37. Warda Hassan, Sajida Noureen, Mujahid Mustaqeem, Tawfik A. Saleh, and Shagufta Zafar, Efficient adsorbent derived from Haloxylon recurvum Plant for the adsorption of Acid Brown dye: Kinetics, isotherm and thermod ynamicoptimization, 2020. *Surfaces and Interfaces*, 100510.